Calibrated nanoscale dopant profiling using a scanning microwave microscope

H. P. Huber, I. Humer, M. Hochleitner, M. Fenner, M. Moertelmaier et al.

Related Articles

Seebeck coefficient of a quantum confined, high-electron-density electron gas in SrTiO3
Appl. Phys. Lett. 100, 161601 (2012)

Improved photoresponsivity of semiconducting BaSi2 epitaxial films grown on a tunnel junction for thin-film solar cells
Appl. Phys. Lett. 100, 152114 (2012)

Few electron double quantum dot in an isotopically purified 28Si quantum well
Appl. Phys. Lett. 100, 143110 (2012)

Fluorinated copper-phthalocyanine/cobalt-phthalocyaine organic heterojunctions: Charge transport and Kelvin probe studies
Appl. Phys. Lett. 100, 142104 (2012)

A sintered nanoparticle p-n junction observed by a Seebeck microscan
J. Appl. Phys. 111, 054320 (2012)

Additional information on J. Appl. Phys.

Journal Homepage: http://jap.aip.org/

Journal Information: http://jap.aip.org/about/about_the_journal

Top downloads: http://jap.aip.org/features/most_downloaded

Information for Authors: http://jap.aip.org/authors

Calibrated nanoscale dopant profiling using a scanning microwave microscope

H. P. Huber,[1] I. Humer,[2] M. Hochleitner,[1] M. Fenner,[3] M. Moertelmaier,[3] C. Rankl,[3]
A. Imtiaz,[4] T. M. Wallis,[4] H. Tanbakuchi,[3] P. Hinterdorfer,[1] P. Kabos,[4] J. Smoliner,[2]
J. J. Kopanski,[5] and F. Kienberger[3,a)]

[1]*University of Linz, Christian Doppler Laboratory for Nanoscopic Methods in Biophysics,
Altenbergerstrasse 69, 4040 Linz, Austria*
[2]*Technical University of Vienna, Institute for Solid State Electronics, 1040 Vienna, Austria*
[3]*Agilent Technologies, Inc., 5301 Stevens Creek Blvd., Santa Clara, California 95051, USA*
[4]*National Institute for Standards and Technology, Electromagnetic Division, 325 Broadway, Boulder,
Colorado 80305-3337, USA*
[5]*National Institute of Standards and Technology, Semiconductor Measurements Division, Gaithersburg,
Maryland 20899-8120, USA*

The scanning microwave microscope is used for calibrated capacitance spectroscopy and spatially resolved dopant profiling measurements. It consists of an atomic force microscope combined with a vector network analyzer operating between 1–20 GHz. On silicon semiconductor calibration samples with doping concentrations ranging from 10^{15} to 10^{20} atoms/cm^3, calibrated capacitance-voltage curves as well as derivative dC/dV curves were acquired. The change of the capacitance and the dC/dV signal is directly related to the dopant concentration allowing for quantitative dopant profiling. The method was tested on various samples with known dopant concentration and the resolution of dopant profiling determined to 20% while the absolute accuracy is within an order of magnitude. Using a modeling approach the dopant profiling calibration curves were analyzed with respect to varying tip diameter and oxide thickness allowing for improvements of the calibration accuracy. Bipolar samples were investigated and nano-scale defect structures and p-n junction interfaces imaged showing potential applications for the study of semiconductor device performance and failure analysis. © *2012 American Institute of Physics*. [doi:10.1063/1.3672445]

I. INTRODUCTION

In scanning microwave microscopy (SMM), a performance network analyzer (PNA) sends a continuous microwave (MW) signal to the conductive tip of an atomic force microscope (AFM).[1] Depending on the impedance of the tip-sample interface, part of the microwave signal is reflected and measured by the PNA as the scattering S11 reflection signal. In SMM, the sample or 'device under test' (DUT referred in network analysis) consists of the AFM probe and the region of the sample immediately beneath the AFM probe tip.[2–4] Scanning capacitance measurements of semiconductors is one promising application of impedance measurements with SMM.[5] Usually an insulating oxide layer of a few angstroms grows on semiconductors like Si or GaAs due to oxygen exposure. Therefore, a conductive AFM tip and the semiconductor form a metal-oxide-semiconductor (MOS) system.[6] Depending on the sign of the applied bias voltage to the tip, the charge carriers in the semiconductor are attracted or depleted from the surface forming a space charge region. The width of the space charge region in the semiconductor varies with the tip bias affecting the capacitance of the MOS junction. For a given tip bias, the width of the space charge region is also a function of the charge car-

rier density in the semiconductor, which is in many cases approximately the concentration of impurity donor or acceptor atoms, i.e. the dopant concentration. Measuring the capacitance difference ΔC of the tip-sample interface and its variation with an applied tip-sample bias is an important extension for the electrical characterization of semiconductors (referred as dC/dV imaging). Recently, it was shown that the reflection coefficient S$_{11}$ amplitude can be calibrated to yield quantitative measurements of the capacitance at the tip sample interface.[7] Calibrated SMM enables a two dimensional mapping of the carrier density across different regions of a semiconductor, with applications in failure analysis, characterization and performance modeling of semiconductor devices.[5,8]

In comparison to SMM, scanning nonlinear dielectric microscopy (SNDM) and scanning capacitance microscopy (SCM) provide information on the differential capacitance of semiconductor materials.[9–12] In SCM, a resonant capacitance sensor is connected to a grounded tip via a transmission line attached to a UHF capacitance sensor. The working frequency of SCM is fixed to ~1 GHz, while SMM can operate in a broad band spectrum typically between 1 MHz and 20 GHz. For the same data acquisition time and capacitance values, higher operating frequencies (ω_{HF}) result in increased load impedance changes in Z$_L$ due to Z ~ 1/jω_{HF}C of the resonator, sample, and shunt resistor combination [Fig. 1(a)]. With the PNA measuring the scattering S$_{11}$ reflection based
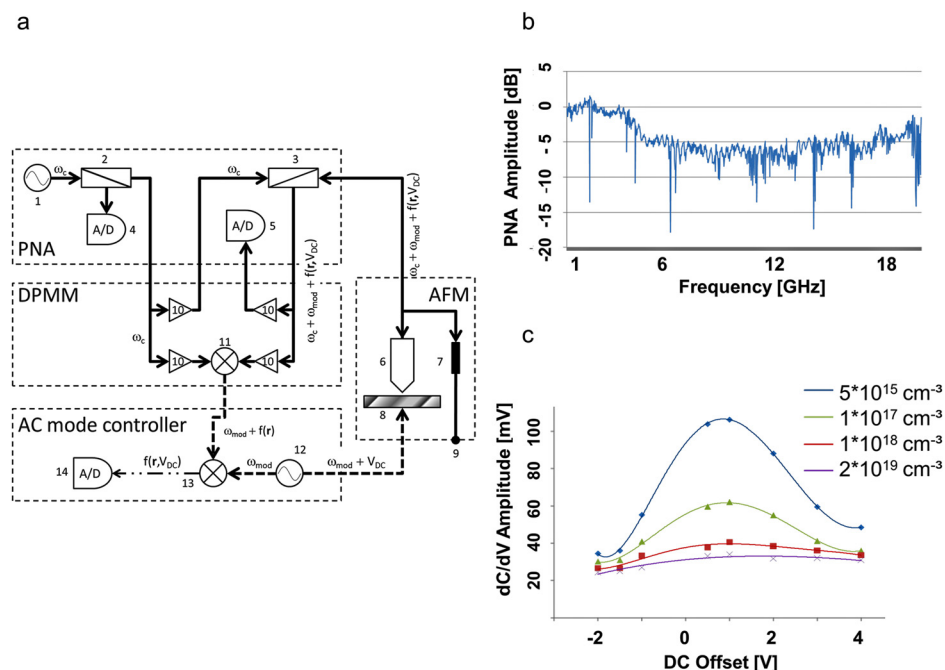
a

b

c

FIG. 1. (Color online) The principle of dopant profiling with scanning microwave microscopy (SMM). (a) The signal pathway for dC/dV imaging using the DPMM (dopant profiling measurement module) and the AC mode controller. 1: Microwave source, 2: directional coupler for power reference, 3: directional coupler for reflected signal power, 4: data acquisition for power reference, 5: data acquisition for reflected signal power, 6: AFM scanner and tip, 7: 50 Ω load in resonator setup with AFM tip, 8: sample, 9: signal ground, 10: MW amplifiers, 11 MW mixer for demodulation, 12: low frequency oscillator, 13: low frequency mixer for demodulating the ω_{mod} signal, 14: dC/dV ($\mathbf{r}$,V_{DC}) data acquisition; (b) PNA amplitude reflection (in Decibel dB) vs signal frequency from 1 to 20 GHz. (c) Spectroscopy curves showing dC/dV amplitude vs DC tip bias on differently doped regions of a n-type semiconductor. The doping levels range from 10^{15} to 10^{19} atoms/cm^3.

on the impedance ($S_{11} = (Z_L - Z_0)/(Z_L + Z_0)$; with Z_L the load impedance and Z_0 the characteristic impedance of the transmission line standardized as 50 Ωs), this impedance change leads to larger changes in the amplitude of the reflection coefficient S_{11} and consequently to improved, frequency controlled, signal-to-noise ratio of SMM. For differential capacitance measurements the modulating AC bias frequency is typically 10 kHz for both SMM and SCM. Sample preparation is important in SCM including a polishing procedure and a stage where the surface oxide is formed and passivated. In SMM, no special oxide preparation is necessary. Recently, a method for quantitative scanning capacitance spectroscopy was introduced with an external capacitance bridge connected to an AFM.[13] The low frequency (1–20 kHz) capacitance bridge is used to measure the local capacitance between the tip and the sample. In this way, capacitance spectroscopy can be carried out with SCM, where the capacitance is recorded during a DC voltage sweep to obtain a capacitance versus voltage C-V curve for further analysis. However, this method is in the order of 100 times slower than C-V curves acquired with SMM.[5]

In this paper, we focus on SMM based C-V spectroscopy and dC/dV imaging of silicon semiconductors with doping concentrations ranging from 10^{15} to 10^{20} atoms/cm^3. A quantitative dC/dV dopant profiling calibration is performed on p- and n-doped samples with known dopant densities. Its limitations were analyzed using a model approach and the accuracy determined by evaluating bipolar SRAM samples.

II. MATERIALS AND METHODS

A. Capacitance measurements

In the reflection mode PNA measurements, the impedance mismatch between the transmission line and the DUT results in a fraction of the incident microwave signal being

back-reflected toward the signal source. A schematic setup is outlined in Fig. 1(a). As the impedances under study are significantly different from the characteristic impedance of the network analyzer, a transformation to 50 Ω is necessary and achieved by using an external 50 Ω shunt. The AFM probe tip is in contact with the sample using a conductive AFM cantilever. A microwave shield was added to the AFM tip holder in order to shield the conductive body of the cantilever from the surrounding environment. For the reported SMM measurements, an Agilent 5400 or 5600 AFM (Agilent Technologies, Chandler, AZ, USA) is combined with an Agilent PNA series network analyzer E8362B (Agilent Technologies, Santa Rosa, CA, USA). Solid metal cantilevers (Rocky Mountain RMN 12Pt 400 A) were used. (*Disclaimer: 'Certain commercial equipment, instruments, or materials are identified in this paper in order to adequately specify the experimental procedure. Such identification does not imply recommendation or endorsement by NIST, nor does it imply that the materials or equipment used are necessarily the best available for the purpose'*). In the SMM capacitance measurement mode, the topographical image is acquired simultaneously with the PNA amplitude/capacitance image. After approaching the AFM-tip to the sample, the S_{11} reflection amplitude and phase versus frequency were acquired. Figure 1(b) shows a typical amplitude frequency dependence from 1–20 GHz. Using the capacitance calibration workflow, the PNA amplitude dB values are transferred to femtoFarad (fF) values.[7] By sweeping over the tip DC bias (typically between -4 and $+4$V) calibrated C-V curves were acquired at fixed lateral positions.

B. dC/dV imaging

For dC/dV imaging, we additionally used a dopant profiling measurement module (DPMM) attached to the PNA and a lock-in modulation technology [see Fig. 1(a)]; the operation is explained in detail in Ref. 14. This measurement technique

requires two signals: a low-frequency (LF) signal (in the kHz to MHz region) to modulate the capacitance of the semiconductor through the native oxide interface and a PNA stimulus signal (1–20 GHz) that passes through the DPMM to the AFM tip as the incident MW signal. Due to changes in the capacitance of the sample induced by the LF signal, the reflected MW signal is modulated at a rate equal to the LF. The signal returned toward the PNA is a superposition of the MW signal in the GHz range and the LF modulation. A multi-step lock-in amplifier (LIA) technique is applied to gain the response of the system to the LF modulation. In a first step, the reflected signal is fed into two amplifiers, one turns the signal back into the PNA for S_{11} measurement and the other one feeds the signal into a mixer where it is superimposed with the continuous MW signal leaving the PNA. This process removes the high frequency MW part of the signal and sends the LF signal to a second lock-in amplifier operating at the modulation frequency. The second lock-in amplifier rectifies the LF signal and generates a DC output signal which is proportional to the LF modulation response of the capacitance. The technique effectively measures the derivative of the C-V curve with respect to the bias voltage at a fixed DC bias. The output signal is therefore referred to as the dC/dV signal. The dC/dV signal generally has a bandwidth up into the kHz range and is suitable to be acquired synchronously to the scanning of the sample surface. The complex dC/dV signal can be plotted either as amplitude and phase images or x- and y-component images; both descriptions contain the same information and are interchangeable.

For the dC/dV imaging a sharp resonance peak in the PNA amplitude spectrum was chosen between 1–20 GHz (typically 19 GHz), and the PNA frequency is adjusted in 2 MHz steps so that an optimal dC/dV amplitude signal is achieved. Then appropriate values for the AC-drive voltage and frequency are chosen, typical values are 0.5 V and 15 kHz, respectively. Figure 1(c) shows dC/dV (V) curves for distinct doping concentrations on n-typed silicon. Those curves are acquired at fixed lateral positions by changing the DC-tip bias. Out of the measured spectra the best tip-bias V_{DC}, e.g., those with the highest dC/dV signal was used for subsequent imaging. Typically, for n-doped samples the maximum signal occurs at positive DC tip bias voltages and for p-doped samples at negative bias voltages. Scan speeds were ~1 line/s with an imaging rate of roughly 8 min/frame (512×512 pixels per frame).

C. Sample description

For our measurements, well characterized dopant profiling calibration samples were used. Those samples are commercially available from IMEC CAMS (Center for Advanced Metrology Solutions), Belgium (part numbers T8_3 and T9 for p-doped and n-doped, respectively). They consist of several layers of silicon with varying dopant density grown on a silicon wafer.[15] The dopants are either donors or acceptors resulting in n- or p-doped material, respectively. The wafers are then cleaved to expose the cross sections of the layers. The local distributions of the dopant concentration in these cross sections have been determined

by a number of complementary techniques and detailed specification sheets have been established.[15] In addition, a p-type sample with known doping concentration as well as a bipolar SRAM (static random access memory) integrated circuit device have been investigated (standard test sample with doping densities given in Ref. 16).

D. FASTC2D modeling

The *FASTC2D* software from NIST[17,18] rapidly converts dC/dV images of dopant gradients in semiconductors to two-dimensional dopant profiles. *FASTC2D* uses a so-called quasi-3D model of the MOS capacitor formed by the tip and an oxidized semiconductor surface. Here the standard 1D model of the MOS capacitor is used to calculate a database of 1D C-V curves. The C-V curve database consists of an array of C-V curves at many different dopant concentrations and oxide thicknesses. The use of a database allows the 3D tip-sample C-V curves to be calculated very rapidly, regardless of the time required to calculate an individual 1D C-V curve. The 3D nature of the tip-semiconductor system is approximated by breaking the tip into a series of 140 concentric rings, parallel and progressively offset from the surface, and then summing the 1D C-V characteristics to simulate the 3D tip-to-sample C-V curve. *FASTC2D* can then calculate the SMM dC/dV response as a function of dopant concentration from the tip C-V curves.

FASTC2D simulates dC/dV response using 3 tip model parameters (tip spherical radius, tip flat radius, and tip shank cone angle), 3 sample model parameters (oxide thickness, oxide dielectric constant, and sample conductivity type), and 3 operating point model parameters (magnitude of the low frequency and high frequency voltages, and the dc operating voltage relative to the sample flatband voltage at one dopant concentration). Initially, the dopant profile is determined from the measured SMM response using the best estimate of all the model parameters and one normalization point of signal at a known dopant concentration (for example, the peak dopant concentration). This normalization point accounts for the difficult to measure tip-to-sample coupling and instrument tuning. If additional information is known about the profile (for example, the substrate concentration or the total dose of an ion implanted profile), the fit of the extracted dopant profile can be improved by slightly adjusting one or more of the model parameters. The goal of tuning the model parameters is to produce a simulation that agrees exactly with measurement at one dopant concentration point and predicts the dopant concentration at all the other points using a physics based model and all the information that is known about the sample. In practice, only the following parameters are adjusted:

1. Oxide dielectric constant-to-oxide thickness (ε_{ox}/t_{ox}) ratio

FASTC2D calculates differential capacitance signal using a one dimensional MOS model and approximates the 3D aspect of the problem by breaking the tip into a series of 140 concentric rings at different tip-sample spacings above the surface. This approach tends to over-estimate the field strength at the surface. Hence we usually get better fits to

experimental data by decreasing the oxide (ε_{ox}/t_{ox}) ratio; that is, by using a fictitiously smaller dielectric constant or larger oxide thickness as model parameters. Adjusting these two parameters changes the total range of the calculated differential capacitance signal over the dopant concentration range. A similar effect can be obtained by reducing the modeled AC and/or HF voltages with respect to the actual applied values.

2. Tip-to-sample flatband voltage

When varying the applied tip DC voltage the differential-capacitance signal should reach a maximum near the flatband voltage. Flatband voltage is also a function of dopant concentration, so that when imaging a dopant gradient sample, the tip will be biased at flatband at only one dopant concentration and all other dopant concentrations will be imaged at a predictable offset from flatband. The dopant concentration where the tip is biased exactly at flatband is an adjustable parameter in *FASTC2D* and this value allows the tip-sample work function and surface charge to be accounted for in the *FASTC2D* model. By varying the tip bias or dopant concentration used by the model as the DC operating point of the measurement, the curvature of the calibration curve, especially at lower dopant concentrations, can be adjusted. Adjusting this parameter may compensate for uncertainties in the applied DC bias relative to the sample flatband voltage, but it also partially compensates for limitations of the quasi-3D model used by *FASTC2D*.

Measured dC/dV signals are converted to dopant concentration through use of the calibration curve method. The calibration curve is determined by calculating the SMM signal for distinct values of dopant concentration using the model parameters for which the SMM data was acquired. The SMM signal value at each x- and y- position of the image is related to a value of dopant concentration from interpolation versus the calibration curve points. Each measured differential capacitance point is treated independently; i.e., the effect of the local dopant gradient and curvature is ignored. Because the adjacent points are not considered, one calibration curve is equally suitable for every point of the entire SMM image.

The quasi-3D model used by *FASTC2D* has a few limitations. While the model reproduces the functional dependence of the dC/dV signal on all the model parameters, it does not produce detailed agreement in the shape of the dC/dV versus tip bias voltage curve for a tip-oxide-silicon measurement, even for uniformly doped material. A full three-dimensional Poisson solution of the SMM/SCM geometry produces dC/dV versus V curves that are a better match to measurement. The quasi-3D model works best when the dopant profile varies a small amount over the scale of the tip radius. *FASTC2D* will not accurately predict dC/dV signal for profiles which change rapidly with respect to tip radius. While the quasi-3D model is relatively insensitive to the tip radius parameter after signal normalization, measurements with tips that are sharp with respect to the profile are necessary to get the best quality results. Finally, the quality of the fit of theory to data depends critically on producing a sample with a high quality oxide (low interface traps and no leakage

current influencing the measured dC/dV) and data acquisition conditions which limit photo generated carriers.

III. RESULTS AND DISCUSSION

A. Calibrated capacitance spectroscopy C-V curves

The PNA measurement frequency was adjusted to $\sim$19 GHz by acquiring the reflection amplitude spectroscopy curve shown in Fig. 1(b). Using the PNA amplitude of the S_{11} reflection coefficient signal, we acquired calibrated C-V curves at different positions on the n- and p-doped calibration samples (Fig. 2). The doping concentration can thereby be evaluated using the relative change of the capacitance in accumulation and depletion regions. For this the tip was located at fixed positions and the tip-bias was swept from roughly -4 to $+4$ V while the PNA amplitude signal was acquired at 19 GHz. The PNA amplitude signals were transferred into fF values by using a capacitance calibration sample which consists of conductive gold pads of various sizes on a SiO_2 staircase structure.[7] The sample capacitance could thereby be described as idealized parallel plates with the SiO_2 dielectric sandwiched in between. From this procedure, a calibration factor Alpha (with units of fF/dB) is determined and used to convert S_{11} (dB) values into capacitance (fF) values. Typical values of Alpha are between 0.2 and 2 fF/dB (depending on tips and parameter settings). Figures 2(a) and 2(b) show C-V curves acquired on regions with different doping concentrations on the n-doped and p-doped
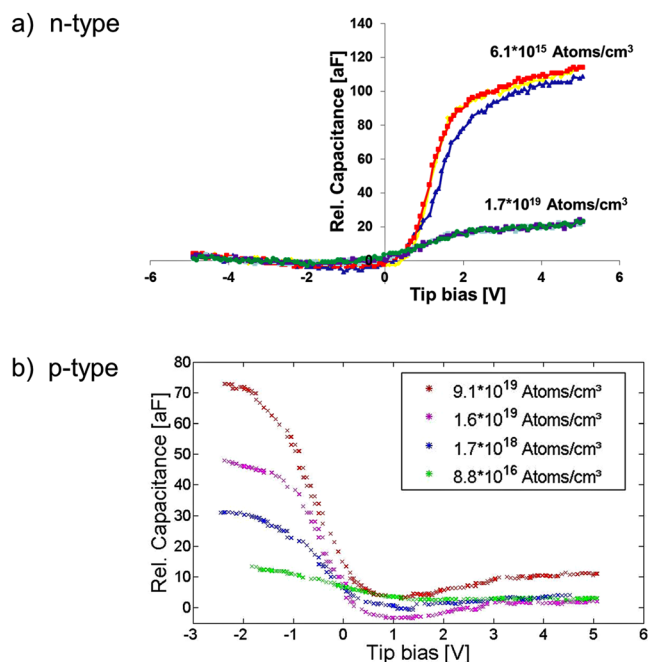
FIG. 2. (Color online) Calibrated C-V curves acquired at 19 GHz on doped semiconductors. (a) On a laterally fixed position on the n-doped sample the PNA amplitude was acquired at different DC-tip bias voltages ranging from -4 to $+4$ V. The reflection amplitude values were calibrated to femto-Farad (fF) using a capacitance calibration sample. C-V curves were acquired at two different positions with different doping concentrations (6.1×10^{15}, 1.7×10^{19} atoms/cm^3) and three curves are shown for each position. (b) C-V measurements (tip bias ranging between -3 and $+3$ V) were done on a p-doped sample on four different positions with different doping concentrations (8.8×10^{16}, 1.7×10^{18}, 1.6×10^{19}, 9.1×10^{19} atoms/cm^3).
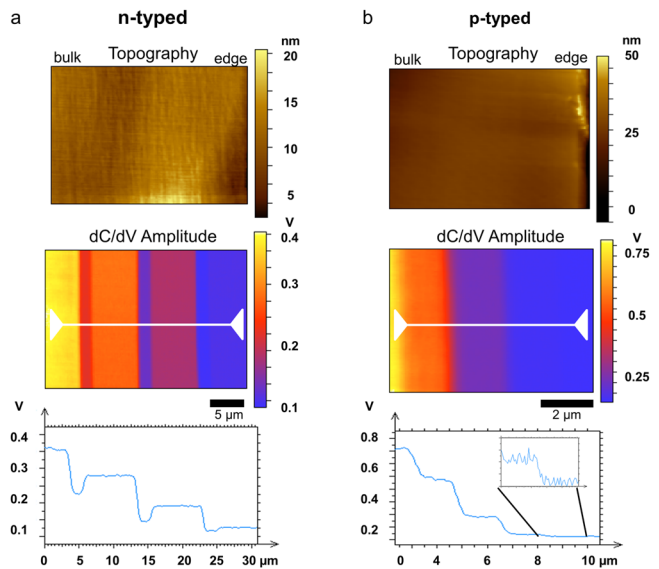
FIG. 3. (Color online) SMM topography (upper panel) and dC/dV images (center panel) of n-typed (left; 30×30 um image size) and p-typed (right; 10×10 um image size) doped semiconductors acquired at 19 GHz and modulation frequency of 14 kHz. DC tip bias was $+1$ and -1 V for n- and p-type, respectively. The lower panel shows the cross section profiles along the white lines. In accordance with the specification sheets four and five distinguished steps can be obtained for the n- doped and p-doped samples, respectively. The edge corresponds to high doping concentration and the bulk to low doping.

calibration samples, respectively. For low doping concentrations ($\sim 10^{16}$ atoms/cm^3) the change of the capacitance with the change of the tip-bias is around 70–120 aF, while for high doping concentrations ($\sim 10^{19}$ atoms/cm^3) the capacitance change is around 10–20 aF.

B. Dopant profiling calibration curves

The dC/dV signal intensity was optimized following the procedure described in Sec. II B, at a fixed AC bias of

$+0.5$ V peak-to-peak amplitude and a modulation frequency of about 15 kHz. The dC/dV (V) curves acquired at different doping concentrations are plotted in Fig. 1(c). Out of these data, the optimal DC tip-bias voltage was selected for subsequent dC/dV imaging. In Figs. 3(a) and 3(b) the topography, as well as the simultaneously recorded dC/dV amplitude images of n- and p-doped calibration samples, are represented. The cross section profiles in Fig. 3 are acquired on the location of the white lines and show a uniform signal in the differently doped regions. As one can see, the topography of both samples is almost flat and does not interfere with the dC/dV measurement. According to the corresponding specification sheets of the calibration samples,[15] the p-doped sample shows dopant concentrations between 1.4×10^{16} (bulk) and 9.1×10^{19} atoms/cm^3 (edge), whereas the doping of the n-type sample ranges from 4.1×10^{15} (bulk) to 1.7×10^{19} atoms/cm^3 (edge). In Fig. 3, the bulk region with the lowest doping concentration is on the left while the highest doping is on the right hand side close to the edge. As follows from MOS theory, a lower doping concentration results in a higher dC/dV amplitude and vice versa.[19] This trend is clearly shown on the cross sectional profile in Fig. 3.

From the dC/dV images of the p- and n-doped calibration samples calibration curves were determined. Using software based analysis of the signals taken in the differently doped regions (PicoImage, Agilent Technologies), average dC/dV amplitude values were calculated and compared to the known dopant concentration from the specification sheet. The so achieved calibration curves are plotted in Figs. 4(a) and 4(b). The plot of the dC/dV signal versus dopant concentration (later referred to the dopant calibration curve) can be used for quantitative evaluation of doping concentrations. While the doping concentrations range from 10^{15} to 10^{20} atoms/cm^3, the corresponding dC/dV amplitude values vary between roughly 0 and 1 V, respectively. The higher the measurement frequency the higher the dC/dV signals and the corresponding signal-to-noise ratio (SNR); e.g.,

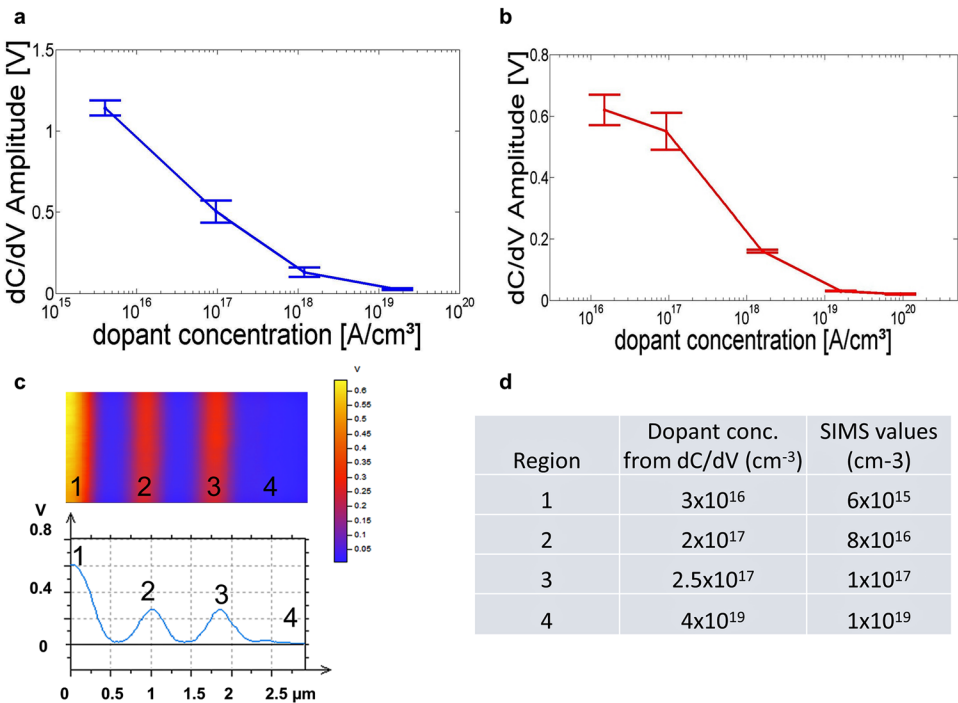| Region	Dopant conc. from dC/dV (cm^{-3})	SIMS values (cm-3)
1	3×10^{16}	6×10^{15}
2	2×10^{17}	8×10^{16}
3	2.5×10^{17}	1×10^{17}
4	4×10^{19}	1×10^{19}

FIG. 4. (Color online) Dopant calibration curves showing the dC/dV amplitude with respect to the dopant concentration for the n-doped (a) and p-doped (b) calibration sample. From the dC/dV images the average amplitude was analyzed at various regions of interests (PicoView software, Agilent Technologies) and plotted with respect to the corresponding doping concentrations as taken from the supplier specification sheets. (c) dC/dV image of a p-doped test sample with four different doping densities: 6×10^{15} (region 1), 8×10^{16} (region 2), 1×10^{17} (region 3), and 1×10^{19} atoms/cm^3 (region 4). The regions 2 and 3 are 300 nm wide. (d) Table comparing doping concentrations based on the dC/dV image and reference values for regions 1–4 (Ref. 19).

on the n-doped calibration sample a $\sim$10 times higher SNR is obtained at 19 GHz compared to 2 GHz (data not shown). Figure 4(c) shows a dC/dV image of a test sample with four different 300 nm wide p-doped areas. According to the measured dC/dV signals and the corresponding calibration curve (acquired with the same set of imaging parameters and the same tip), the dopant concentration was determined for the four different regions. The results were compared to the data from SIMS (secondary ion mass spectrometry) and are listed in Fig. 4(d). It was found that the absolute SMM values agree within an order of magnitude to the absolute SIMS data. Regarding resolution, two differently doped areas can be distinguished (e.g., region 2 and 3) if there dopant density is 20% different.

For proper comparison of dC/dV signals between calibration sample and 'unknown' sample, it is crucial to keep the imaging parameters like PNA frequency and AC-drive constant. However, there are several additional factors related to non-uniform sample properties that influence the accuracy of the calibration procedure. Uncertainties are introduced mainly from varying quality of tip-sample junctions, contamination of the sample surface and changes of the insulator thickness of the MOS junction. These effects lead to different slopes in the C-V curves and therefore to varying dC/dV signals. When comparing unknown samples to calibration samples, variations of the oxide thickness may influence the accuracy by the same effect. From several test measurements where imaging parameters, tips, and samples have been varied and investigated over time we determined the repeatability and accuracy of evaluating absolute doping concentrations. Within a dynamic range of 10^{15} to 10^{20} atoms/cm^3 absolute doping concentrations can be evaluated within an order of magnitude on untreated samples with native oxide. Relative doping concentrations can be measured with a much better resolution of $\sim$20%, though. Relative dopant profiling is particularly useful when differently doped regions need to be distinguished on the same sample or when a reference spot with known dopant density is available. Furthermore, different tips with varying diameters and shapes result in different calibration curves.[20] Therefore, the calibration has to be repeated when, e.g., cantilevers are changed. Overall, the use of specially prepared samples with a defined thickness of the oxide surface can significantly increase the measurement accuracy.[10] More insights into the sensitivity and reproducibility of the calibration procedure can be gained when the various effects (e.g., varying oxide thickness) are modeled and their influence on the calibration curves studied in the next chapter.

C. Dopant profiling and capacitance spectroscopy modeling

FASTC2D was used to model the differential capacitance versus voltage, and calibration curve data taken with the SMM. Experimentally, some of the *FASTC2D* model parameters are known precisely and others are educated guesses. To improve the fit of the theoretical differential capacitance simulations to experimental data, a calibration curve is first calculated using the best known values of the measurement parameters and one normalization point, where both the differential capacitance signal magnitude and dop-

ant concentration are known. Adjustable model parameters include the tip shape (radius of curvature and cone angle), sample parameters (conduction type, surface insulator thickness, t_{ox}, and dielectric constant, ε_{ox}), the SMM operating point (applied DC bias relative to flatband, magnitudes of the applied AC and HF voltages), and a normalization point (signal level at one known dopant concentration).

FASTC2D fits to the differential capacitance versus voltage curves from Fig. 1(c) are shown in Fig. 5(a), fits to the n-type calibration curve from Fig. 4(a) are shown in Fig. 5(b), and fits to the p-type calibration curve from Fig. 4(b) are shown in Fig. 5(c). In Fig. 5(a), relatively good agreement is made between the measured and modeled dC-V curves by increasing the value of the HF voltage, which tends to broaden the peaks in dC. Flatband point of the modeled dC-V curves is shifted by $+0.8$ V to align the flatband voltage with the experimental data. The relative magnitudes of the measured dC-V curves are in approximate agreement with the modeled values.

Two fits are shown for the n-type calibration curve in Fig. 5(b). The solid black line is a fit with all model parameters at their nominal values and the dashed black line with a fictitiously large value of (ε_{ox}/t_{ox}). Three fits are shown for the p-type calibration curves in Fig. 5(c). The solid black line shows the first fit with all model parameters at their nominal values. The quality of the fit was improved by decreasing the value of (ε_{ox}/t_{ox}) and by varying the modeled DC operating point of the SMM with respect to the surface flatband condition (dashed and dotted lines). Both of the fits with fictitious parameters are equally good, though the fit with (ε_{ox}/t_{ox}) = 0.5 probably reflects the curvature of the calibration curve better. The level of variation of the model parameters used in *FASTC2D* to fit model response to experimental data is in keeping with those previous seen for SCM using an RCA style sensor.[21,22] With respect to its agreement with the FASTC2D modeling software, the SMM seems to be measuring the same physical quantities as the SCM.

D. Dopant profiling on a bipolar p-n sample

In addition to unipolar doped samples, a conventional bipolar p-n SRAM sample has been investigated and dC/dV images acquired after optimization of the PNA frequency to $\sim$18 GHz and the low frequency modulation to 14 kHz at 1 V AC bias. A topographic image of the investigated sample is shown in Fig. 6(a) including a sketch correlating the topographic features with doping type and corresponding concentrations listed in Fig. 6(d).[16,23] The schematic indicates p-type areas with reference doping concentrations ranging from 2×10^{16} to 2×10^{17} atoms/cm^{-3} (p-epi, p-doped channel) and n-type areas ranging from 5×10^{18} to 2×10^{20} atoms/cm^{-3} (n+, n-LDD). Figure 6(b) shows the dC/dV phase image; the various n- and p-doped areas can be distinguished and no cross-talk with the topography is observed. To separate between n- and p-type doping the complex dC/dV signal has been analyzed and four specifically selected areas were plotted in a scatterplot [Fig. 6(c)]. Note that the complex dC/dV signal can be analyzed either in the frame of amplitude/phase or x/y components, both representations contain the same information and are interchangeable. By changing the phase the measurement can be adjusted so that
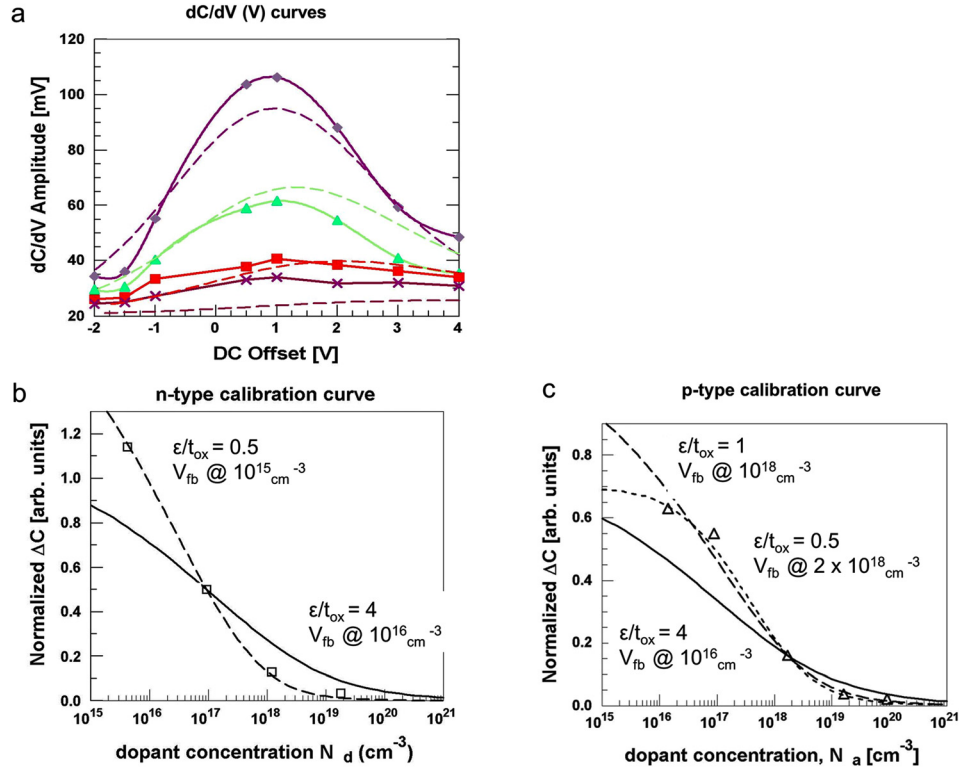
FIG. 5. (Color online) Modeling of SMM data using *FASTC2D*. (a) *FASTC2D* fit to the experimentally measured dC/dV (V) curves shown in Fig. 1(c). The qualitative behavior at different dopant densities can be properly described. All model parameters are the same as their experimental values, except for the magnitude of the high frequency voltage which was allowed to vary from the estimated 800 mV actually applied to 3000 mV. (b) *FASTC2D* fits to the experimentally determined n-type calibration curve shown in Fig. 4(a). Normalization point for all fits is 0.5 at $N_d = 9.4 \times 10^{16}$ cm^{-3}. Solid black line is a fit with all model parameters at their nominal values, $(\varepsilon_{ox}/t_{ox}) = (3.9/1 \text{ nm}) = 3.9$, and the DC bias tuned to produce the maximum dC response at $N_d = 10^{16}$ cm^{-3}. Dashed black line is a fit with $(\varepsilon_{ox}/t_{ox}) = 0.5$ and the DC bias tuned to produce the maximum response at $N_d = 10^{15}$ cm^{-3}. (c) *FASTC2D* fits to the experimentally determined p-type calibration curve shown in Fig. 4(b). Normalization point for all fits is 0.16 at $N_a = 1.7 \times 10^{18}$ cm^{-3}. Solid black line is a fit with all model parameters at their nominal values, $(\varepsilon_{ox}/t_{ox}) = (3.9/1 \text{ nm}) = 3.9$ and the DC bias tuned to produce the maximum dC response at $N_a = 10^{16}$ cm^{-3}. Dashed black line is a fit with $(\varepsilon_{ox}/t_{ox}) = 0.5$ and the DC bias tuned to produce the maximum response at $N_a = 2 \times 10^{18}$ cm^{-3}. Dotted black line is a fit with $(\varepsilon_{ox}/t_{ox}) = 1.0$ and the DC bias tuned to produce the maximum response at $N_a = 1 \times 10^{18}$ cm^{-3}.

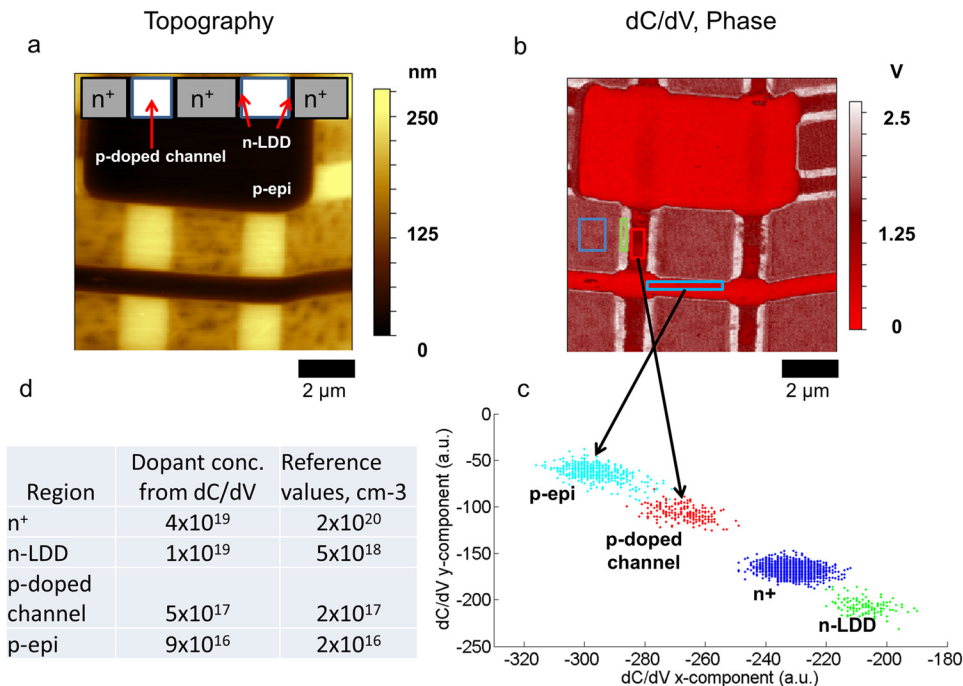| Region	Dopant conc. from dC/dV	Reference values, cm-3
n+	4×10^{19}	2×10^{20}
n-LDD	1×10^{19}	5×10^{18}
p-doped channel	5×10^{17}	2×10^{17}
p-epi	9×10^{16}	2×10^{16}

FIG. 6. (Color online) dC/dV imaging of a hetero-bipolar SRAM sample and estimation of doping concentration. (a) Topographical image with 10×10 μm scan size and sketch of the differently doped regions. (b) Simultaneously acquired dC/dV phase image. From the data points within the labeled squares a scatterplot of the dC/dV x and y components is shown in (c). The various regions of interest (p-epi, p-doped channel, n+, n-LDD) can be clearly distinguished and the doping polarity and density analyzed. (d) The dC/dV signals were transferred to dopant concentrations via the calibration curve and compared to published reference values (Ref. 16).
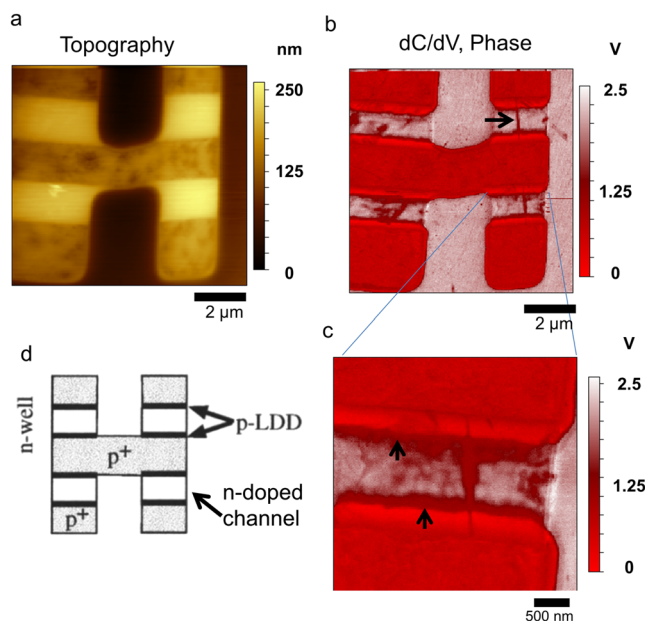
FIG. 7. (Color online) Imaging defect structures and p-n junctions at smaller scale. (a) Topographical image with 10×10 um scan size with sketch of the doping polarities and concentrations in (d) taken from Ref. 16. (b) Corresponding dC/dV phase image with defect structures in the n-doped channels (cf., arrow). (c) dC/dV image with a scan area of 2×2 μm provides a closer look at the n-doped channel and p-n junction interfaces (cf., arrows).

the SMM measures either the component of the signal in-phase or 180 degrees out of phase with respect to the drive signal. For evaluating the doping concentrations dC/dV imaging has been carried out subsequently at a DC tip bias of -0.5 and $+0.5$ V for proper p- and n-type imaging, respectively. By reading out the dC/dV signals of the four selected regions the doping concentrations were looked up in the corresponding p- and n-type calibration curves. The doping levels determined in this manner are compared with the published specification values listed in Fig. 6(d). Overall, absolute doping concentrations correlate between SMM and SIMS reference values within an order of magnitude. Figure 7 shows a more detailed topography and dC/dV image of the SRAM sample. One can identify several p-n defect structures in the n-doped channels observed in the dopant profiling image [cf. arrow in Fig. 7(b)]. A sketch depicts p- and n-doped areas in Fig. 7(d), which corresponds well to the various doping types and concentrations in the dC/dV image. No cross talk is obtained between topography and dopant profiling image. Bipolar p/n junction interfaces are observed with a width of $\sim$100 nm [cf. arrows in Fig. 7(c)]. The exact width of the p-n junction depends on the tip-bias (data not shown) and was investigated in Refs. 16 and 23.

IV. CONCLUSION

The SMM allows for simultaneous topography imaging, capacitance imaging and dC/dV imaging of semiconductor samples at nanoscale resolution. Different doping levels were evaluated using capacitance S_{11} imaging with calibrated C-V curves acquired quickly within seconds at frequencies up to 20 GHz with a sensitivity of $\sim$1 aF. Using specified dopant samples, differential dC/dV imaging allows for the determination of calibration curves for the quantita-

tive evaluation of semiconductor dopant concentrations. The accuracy for dopant profiling is limited to an order of magnitude mostly by varying sample properties like oxide thickness and oxide charging. However, relative doping profiling can be done with $\sim$20% resolution. The calibration can be improved if modeling is included that allows to compensate for changes in, for example, tip-diameter and oxide thickness. Bipolar SRAM samples have been investigated and the p- and n-doping concentrations evaluated. Nanoscale defect structures and p-n junction interfaces were obtained in dC/dV imaging giving relevant insights into semiconductor device performance and failure analysis.

In summary, the SMM is a versatile tool to investigate semiconductor dopant profiling and capacitance spectroscopy at microwave frequencies with nanoscale resolution. The maximum lateral resolution has not yet been determined, since the samples investigated only demonstrate that the resolution is below 100 nm. Experiments to investigate the ultimate doping density dynamic range, the ability to resolve areas of different doping density, and the maximum achievable lateral resolution are currently under way using specially constructed calibration samples.

[1] A. Karbassi, D. Ruf, A. D. Bettermann, C. A. Paulson, D. W. van der Weide, H. Tanbakuchi, and R. Stancliff, Rev. Sci. Instr. **79**, 094706 (2008).
[2] K. Lai, M. B. Ji, N. Leindecker, M. A. Kelly, and Z. X. Shen, Rev. Sci. Instr. **78**, 063702 (2007).
[3] K. Lai, W. Kundhikanjana, M. Kelly, and Z. X. Shen, Rev. Sci. Instr. **79**, 063703 (2008).
[4] T. M. Wallis, A. Imtiaz, H. T. Nembach, P. Rice, and P. Kabos, AIP Conf. Proc. **931**, 525 (2007).
[5] J. Smoliner, H. P. Huber, M. Hochleitner, M. Moertelmaier, and F. Kienberger, J. Appl. Phys. **108**, 064315 (2010).
[6] G. Gomila, J. Toset, and L Fumagalli, J. Appl. Phys. **104**, 024315 (2008).
[7] H. P. Huber, M. Moertelmaier, T. M. Wallis, C. J. Chiang, M. Hochleitner, A. Imtiaz, Y. J. Oh, K. Schilcher, M. Dieudonne, J. Smoliner, P. Hinterdorfer, S. J. Rosner, H. Tanbakuchi, P. Kabos, and F. Kienberger, Rev. Sci. Instr. **81**, 113701 (2010).
[8] A. Imtiaz, S. M. Anlage, J. D. Barry, and J. Melngailis, Appl. Phys. Lett. **90**, 143106 (2009).
[9] C. C. Williams, J. Slinkman, W. P. Hough, and H. K. Wickramasinghe, Appl. Phys. Lett. **55**, 1662 (1989).
[10] J. Isenbart, A. Born, and R. Wiesendanger, Appl. Phys. A: Mater. Sci. Proc. **72**, 243 (2001).
[11] I. Humer, O. Bethge, M. Bodnarchuk, M. Kovalenko, M. Yarema, W. Heiss, H. P. Huber, M. Hochleitner, P. Hinterdorfer, F. Kienberger, J. Smoliner, S. Wu, J.-J. Yu, T. M. Wallis, A. Imtiaz, H. T. Nembach, P. Rice, and P. Kabos, J. Appl. Phys. **109**, 064313 (2011).
[12] K. Honda, K. Ishikawa, and Y. Cho, J. Phys.: Conf. Series **209**, 012050 (2010).
[13] W. Brezna, M. Schramboeck, A. Lugstein, S. Harasek, H. Enichlmair, E. Bertagnolli, E. Gornik, and J. Smoliner, Appl. Phys. Lett. **83**, 4253 (2003).
[14] H. Tanbakuchi, M. Richter, F. Kienberger, and H. P. Huber, *Nanoscale materials and device characterization via a scanning microwave microscope*, IEEE COMCAS 2009, Tel Aviv, Israel.
[15] T. Clarysse, M. Caymax, P. De Wolf, T. Trenkler, W. Vandervorst, J. S. McMurray, J. Kim, C. C. Williams, J. G. Clark, and G. Neubauer, J. Vac. Sci. Tech. B: Microelectronics and Nanometer Structures **16**, 394 (1998).

[16]M. W. Nelson, P. G. Schroeder, R. Schlaf, and B. A. Parkinson, Electrochemical and Solid-State Letters **2**, 475 (1999).

[17]J. J. Kopanski, J. F. Marchiando, and J. R. Lowney, Mater. Sci. Eng. B-Solid State Mater. Adv. Tech. **44**, 46 (1997).

[18]J. F. Marchiando, J. J. Kopanski, and J. R. Lowney. in *Model database for determining dopant profiles from scanning capacitance microscope measurements*, J. Vac. Sci. Technol. B **16**, 463 (1998).

[19]J. Smoliner, B. Basnar, S. Golka, E. Gornik, B. Löffler, M. Schatzmayr, and H. Enichlmair, Appl. Phys. Lett. **79**, 3182 (2001).

[20]C. Eckhardt, W. Brezna, O. Bethge, E. Bertagnolli, and J. Smoliner, J. Appl. Phys. **105**, 113709 (2009).

[21]J. J. Kopanski, J. F. Marchiando, J. Albers, and B. G. Rennex, Characterization and Metrology for ULSI Technology, D. G. Seiler, A. C. Diebold, W. M. Bullis, T. J. Shaffner, R. McDonald, and E. J. Walters, Eds. (AIP, New York, 1998), pp. 725–729.

[22]J. F. Marchiando, J. J. Kopanski, and J. Albers, J. Vac. Sci. Technol. B **18**, 414 (2000).

[23]C. Baumgart, A.-D. Müller, F. Müller, and H. Schmidt, Phys. Status Solidi (a) **208**, 777 (2011).